

1 **Title page**

2 Nutritional inter-dependencies and a carbazole-dioxygenase are key elements of a bacterial  
3 consortium relying on a *Sphingomonas* for the degradation of the fungicide thiabendazole

4

5 Vasileiadis Sotirios <sup>a</sup>, Perruchon Chiara <sup>a</sup>, Scheer Benjamin <sup>b</sup>, Adrian Lorenz <sup>b,d</sup>, Steinbach Nicole <sup>c</sup>,  
6 Trevisan Marco <sup>e</sup>, Plaza-Bolaños Patricia <sup>f</sup>, Agüera Ana <sup>f</sup>, Chatzinotas Antonis <sup>c</sup>, Karpouzas G  
7 Dimitrios <sup>\*a</sup>

8

9 <sup>a</sup>Department of Biochemistry and Biotechnology, Laboratory of Plant and Environmental  
10 Biotechnology, University of Thessaly, Larissa, 41500-Viopolis, Greece

11 <sup>b</sup>Department of Isotope Biogeochemistry and <sup>c</sup>Department of Environmental Microbiology,  
12 Helmholtz Centre for Environmental Research – UFZ, Leipzig, Germany

13 <sup>d</sup>Chair of Geobiotechnology, Technische Universität Berlin, Germany

14 <sup>e</sup>Department of Sustainable Food Process, Università Cattolica del Sacro Cuore, Piacenza, Italy

15 <sup>f</sup>Solar Energy Research Centre (CIESOL), Joint Center University of Almería-CIEMAT, Almería,  
16 Spain

17

18 \*Corresponding Author:

19 Karpouzas DG, University of Thessaly

20 [dkarpouzas@uth.gr](mailto:dkarpouzas@uth.gr)

21

22 **Abstract**

23 **Background:** Thiabendazole (TBZ), is a benzimidazole fungicide and anthelmintic whose high  
24 persistence and toxicity pose a serious environmental threat. In our quest for environmental mitigation  
25 we previously isolated the first TBZ-degrading bacterial consortium and provided preliminary evidence  
26 for its composition and the degrading role of a *Sphingomonas*. Here, we employed a multi-omic  
27 approach combined with DNA-stable isotope probing (SIP) to determine the genetic make-up of the  
28 key consortium members, to disentangle nutritional and metabolic interdependencies, to identify the  
29 transformation pathway of TBZ and to understand the genetic network driving its transformation.

30 **Results:** Time-series SIP in combination with amplicon sequencing analysis verified the key role of  
31 *Sphingomonas* in TBZ degradation by assimilating over 80% of the <sup>13</sup>C-labelled phenyl moiety of TBZ.  
32 Non-target mass spectroscopy (MS) analysis showed the accumulation of thiazole-4-carboxamide as  
33 a single dead-end transformation product and no phenyl-containing derivative, in line with the phenyl  
34 moiety assimilation in the SIP analysis. Time series metagenomic analysis of the consortium  
35 supplemented with TBZ or succinate led to the assembly of 18 metagenome-assembled genomes  
36 (MAGs) with >80% completeness, six (*Sphingomonas* 3X21F, *γ-Proteobacterium* 34A,  
37 *Bradyrhizobiaceae* 9B and *Hydrogenophaga* 19A, 13A, and 23F) being dominant. Meta-transcriptomic  
38 and -proteomic analysis suggested that *Sphingomonas* mobilize a carbazole dioxygenase (*car*) operon  
39 during the initial cleavage of TBZ to thiazole-4-carboxamide and catechol, the latter is further  
40 transformed by enzymes encoded in a catechol *ortho*-cleavage (*cat*) operon; both operons being up-  
41 regulated during TBZ degradation. Computational docking analysis of the terminal oxygenase  
42 component of *car*, CarAa, showed high affinity to TBZ, comparable to carbazole, reinforcing its high  
43 potency for TBZ transformation. These results suggest no interactions between consortium members in  
44 TBZ transformation, performed solely by *Sphingomonas*. In contrast, gene expression network analysis  
45 revealed strong interactions between *Sphingomonas* MAG 3X12F and *Hydrogenophaga* MAG 23F,  
46 with *Hydrogenophaga* activating its cobalamin biosynthetic pathway and *Sphingomonas* its cobalamin  
47 salvage pathway along TBZ degradation.

48 **Conclusions:** Our findings suggest interactions between consortium members which align with the  
49 "black queen hypothesis": *Sphingomonas* detoxifies TBZ, releasing consortium members by a toxicant;  
50 in return for this, *Hydrogenophaga* 23F provides cobalamin to the auxotrophic *Sphingomonas*.

51 **Keywords:** thiabendazole, biodegradation, B12 auxotrophy, bacterial consortium, *Sphingomonas*,  
52 *Hydrogenophaga*, carbazole dioxygenase

## 54 **Background**

55 Thiabendazole (TBZ) is a benzimidazole compound which is used as a post-harvest fungicide to control  
56 fungal infestations on fruits during storage [1] and as a broad spectrum anthelmintic to control  
57 endoparasites in livestock farming [2]. It acts by binding to tubulin monomers inhibiting the  
58 polymerization of microtubules and, thus, cell growth [3-5]. TBZ has been identified as a common  
59 contaminant of natural water resources in citrus producing areas [6, 7] threatening the integrity of water  
60 ecosystems due to its high aquatic toxicity (i.e. NOEC fish = 12  $\mu\text{g L}^{-1}$ ) [8]. We recently reported TBZ  
61 concentration levels in soils adjacent to fruit packaging plants of up to 12,000  $\text{mg kg}^{-1}$  resulting in a  
62 depleted bacterial diversity [9]. The extensive environmental contamination by TBZ is the result of its  
63 high persistence ( $DT_{50(\text{soil} - \text{aerobic})} > 365$  days) [10] and the lack of implemented methods for the treatment  
64 of TBZ-contaminated agro-industrial effluents (despite the implementation of relevant EC legislation)  
65 [11]. The problem is further exemplified by the limited capacity of microbial communities in municipal  
66 wastewater treatment plants to remove recalcitrant chemicals like TBZ [12]. Instead municipal  
67 wastewater treatment plants act as point sources for the contamination of receiving water bodies [12]  
68 and agricultural soils [13]. In the latter case the application of biosolids, derived from a TBZ-containing  
69 wastewater treatment plant, as fertilizers resulted in the persistence of 83% of the initially applied TBZ  
70 after 3 years [13].

71  
72 Bacterial specialists that have the capacity to degrade TBZ could be invaluable in bioaugmentation and  
73 biodepuration strategies to avert its environmental impact. In this context, we recently enriched from a  
74 heavily TBZ contaminated soil the first bacterial consortium capable of degrading and detoxifying TBZ  
75 while using it as the sole carbon source [14, 15]. The consortium, which was dominated by different  $\alpha$ -

76 ,  $\beta$ - and  $\gamma$ -*Proteobacteria*, was stable in its composition and its degrading efficiency. Preliminary assays  
77 (i.e. stable isotope probing combined with denaturant gradient gel electrophoresis (SIP-DGGE)  
78 analysis) pointed to a *Sphingomonas* as the key degrader of TBZ [14], with the roles of the other  
79 consortium members remaining unknown. No single TBZ-degrading bacterial strain was isolated from  
80 the consortium despite our copious attempts with different media and solidifying agents, indicating  
81 underlying interactions of the key degrader with the other members of the consortium. The coherence  
82 of pollutant-degrading microbial consortia goes beyond simple collaborative transformation of the  
83 target pollutants [16, 17] and involves syntrophic and cross-feeding relationships on biomolecules like  
84 amino acids and vitamins [18-20]. Comparative genomic analyses suggested an evolutionary drift in  
85 bacterial genomes towards auxotrophic lifestyles on energetically costly amino acids and cofactors like  
86 B12 [21, 22], shaping microbial communities in various environments and the human gut [23].

87

88 A prerequisite for the biotechnological exploitation of microbial consortia is to disentangle the roles of  
89 keystone members, degraders and suppliers/feeders on key nutrients, whose presence guarantees  
90 consortium coherence [24, 25]. In the current study we seek answers to the following questions: (i) Is  
91 *Sphingomonas* the sole member of the consortium involved in the transformation of TBZ or are there  
92 transformation interdependencies driving the detoxification the fungicide? (ii) Which are the main  
93 transformation products of TBZ? (iii) Which is the role of other members of the consortium, with  
94 respect to TBZ degradation, and does its stable composition infer established roles amongst them? (iv)  
95 Which are the genes and enzymes involved in the transformation process? To answer these questions  
96 we employed, in time series experiments, an integrated, multi-omics approach (meta-  
97 genomics/transcriptomics/proteomics) combined with non-target mass spectroscopy (MS) analysis and  
98 SIP-based amplicon sequencing, with the latter enabling the confident identification of the key  
99 degrading members of the consortium.

100

## 101 **Methods**

### 102 **Microbial consortium growth conditions.**

103 The TBZ-degrading bacterial consortium was routinely grown at 27°C in a minimal salts medium  
104 (MSMN) supplemented with TBZ (25 mg l<sup>-1</sup>) as the sole carbon source [14] (see the supporting  
105 information - SI - for media composition).

106

### 107 **TBZ degradation assays**

108 **Experiment 1 - SIP analysis:** A first degradation assay was performed to identify the members of the  
109 consortium involved in the transformation of TBZ via DNA-SIP based amplicon sequencing analysis.  
110 Triplicate 30-ml cultures of the consortium were supplemented with 25 mg l<sup>-1</sup> of unlabelled (<sup>12</sup>C) or  
111 <sup>13</sup>C-TBZ labelled uniformly in its phenyl moiety (Clearsynth<sup>®</sup>, Mumbai, India). Triplicate flasks of  
112 MSMN supplemented with unlabelled TBZ but not inoculated with the consortium were co-incubated  
113 as abiotic controls. Aliquots of the cultures (0.5 ml) were removed at 36, 72, 117 and 141 h,  
114 (corresponding to 10%, 30%, 100% degradation of TBZ and 24 h after its complete degradation, Figure  
115 1A) to determine: (i) TBZ degradation via HPLC analysis as described previously [14] and (ii)  
116 community composition via DNA extraction and amplicon sequencing as described below.

117 **Experiment 2 - multi-omic analyses:** A second degradation assay was employed to disentangle  
118 metabolic interactions between consortium members and to identify, *via* a multi-omic approach, the  
119 key genes/enzymes driving the transformation of TBZ. Triplicate cultures of the consortium were  
120 amended either with 25 mg l<sup>-1</sup> TBZ (125 µM) or 37 mg l<sup>-1</sup> of succinate (SUC; 314 µM) as the sole  
121 carbon source (with a carbon concentration of 15 µg ml<sup>-1</sup> in each case). Parallel triplicate abiotic  
122 controls as described above were also included. Aliquots (0.5 to 4 ml depending on the type of  
123 measurement employed) were removed from cultures at multiple time points along the degradation of  
124 TBZ and used for DNA/RNA/protein extraction and downstream metagenome binning, transcriptomic,  
125 proteomic and non-target MS analysis for TBZ transformation product detection.

126

### 127 **Nucleic acids extraction and quantification.**

128 DNA and RNA were extracted from bacterial cell pellets with the NucleoSpin<sup>®</sup> Tissue and RNA kits,  
129 respectively (Macherey-Nagel & Co, Düren, Germany). Nucleic acid extracts were quantified with the

130 Quant-iT™ HS ds-DNA assay kit and the Quanti-iT™ RNA HS kit with a Qubit™ fluorometer  
131 (Invitrogen, USA).

132

### 133 **SIP analysis.**

134 DNA extracts from the <sup>13</sup>C-labelled TBZ-treated culture were separated into <sup>13</sup>C-labelled and unlabelled  
135 fractions according to their buoyant density in a CsCl gradient established by ultracentrifugation at  
136 167,000  $\times$  g for 36 hours at 20 °C [26]. DNA was extracted from the CsCl gradient buffer by  
137 glycogel/PEG precipitation and used for subsequent 16S rRNA gene diversity analysis as described  
138 further on and detailed in the SI.

139

### 140 **Amplicon sequencing analysis.**

141 The composition of the bacterial consortium in experiment 1 (SIP), was determined via multiplex  
142 sequencing of PCR amplicons of the V4 hypervariable region of the 16S rRNA gene according to our  
143 in-house protocol [27, 28] using primers 515F/806R [29, 30] as described in details in the SI. The  
144 sample-wise-demultiplexed/quality-controlled read pairs were used for reconstructing the amplicon  
145 sequences which were processed with the Lotus v1.58 suit [31] for generating the 97% sequence identity  
146 operational taxonomic unit (OTU) matrices and obtaining their taxonomic classifications. The  $\beta$ -  
147 diversity analysis was performed with the Entropart v1.4-7 [32] and the Vegan v2.5-5 [33] R v3.6.0  
148 software [34] packages (more details are available in the SI).

149

### 150 **Metagenome assembly, contig binning, annotation and synteny analysis.**

151 Metagenome assembly within the context of the multi-omics experiment 2, was performed using the  
152 sequencing data of five shotgun libraries over three sequencing runs using both second (Illumina) and  
153 third generation (Pacific Biosciences) sequencing approaches as described in detail in the SI. The use  
154 of both second and third generation sequencing approaches along with the choice of samples of the  
155 consortium for DNA extraction at varying experimental conditions (assuring for differential genomic  
156 coverage by the sequencing reads), aimed at achieving a robust assembly of the metagenome and  
157 extracting metagenome assembled genomes (MAGs) as proposed previously [35]. Sequences were

158 quality controlled and the devoted sequencing effort was assessed with Nonpareil v3.301 [36, 37].  
159 Hybrid assembly was performed with Mira v5. 1 [38] and Megahit v1.1.3 [39] as described in the SI.  
160 Metawatt v3.5.3 [40] was used for obtaining MAGs which were further classified and quality assessed  
161 with MiGA against its registered NCBI genome collection [41]. Annotation of the sequences was  
162 performed with Prokka v1.12 [42], enriched with the aromatic hydrocarbon degradation AromaDeg  
163 [43] and the mobile genetic elements ALCME v0.4 [44] protein databases. The predicted open reading  
164 frames (ORFs) were also compared against the SEED database [45] with Rapsearch v2.22 [46]. BLAST  
165 was used for identifying molecular anchors during comparative genomics and the GenoPlotR v0.8.9  
166 [47] R package was used for generating the associated plots.

167

### 168 **RNA sequencing analysis.**

169 Samples from experiment 2 obtained at 57, 73, and 109 hours post inoculation (hpi), corresponding to  
170 40% degradation, 100% degradation and 36 h after 100% degradation of TBZ, were collected from  
171 TBZ amended bacterial cultures (and from the succinate amended cultures) for transcriptomic analysis  
172 via shotgun sequencing in Illumina Hiseq 2x250 bp rapid mode. Quality controlled sequences obtained  
173 were mapped against the reference metagenome assembly sequence with STAR v020201 [48], while  
174 transcript counts were predicted with HTSeq v0.9.1 [49]. Differential expression analysis was  
175 performed using the trimmed mean of M-values (TMM) normalization approach [50] with edgeR  
176 v3.14.0 [51] and hypotheses were tested with the negative binomial models and the generalized linear  
177 model quasi likelihood F-test [52]. Associated multivariate analysis and modeling was performed with  
178 the Vegan R package, while Spearman correlation tests ( $\rho \geq 0.5$ ; Benjamini-Hochberg adjusted P-value  
179  $\leq 0.05$ ) followed by network analysis and associated substructure [53] identification methods were used  
180 for identifying transcript memberships (see SI). Network and the keystone [54] analyses were  
181 performed with Igraph v1.0.1 [55].

182

### 183 **Metaproteomic analysis.**

184 Lysed cells from the same samples used for RNA sequencing were treated with dithiothreitol as  
185 reducing agent and iodoacetamide to break and prevent the reformation of disulfide bonds respectively.

186 The resulting protein extracts were digested with trypsin, and the samples were desalted with ZipTips  
187 as described in detail in the SI. Peptide mixtures were analyzed by nanoLC-MS/MS using an Orbitrap  
188 Fusion mass spectrometer (ThermoFisher Scientific, Waltham, MA, USA). Protein identification was  
189 performed as described previously [56] with Proteome Discoverer v2.2 (ThermoFisher Scientific,  
190 Waltham, MA, USA) using SequestHT to search against the consortium metagenome translations of  
191 the predicted ORFs. Label-free quantification of peptides was done with the Minora node implemented  
192 in Proteome Discoverer. The abundances of confidently predicted proteins (false discovery rate below  
193 1% as determined with the Percolator node) were analysed similarly with the RNA sequencing data  
194 (see SI).

195

#### 196 **Non-target MS analysis of TBZ transformation products.**

197 Samples from experiment 2 collected from different time points along the degradation of TBZ were  
198 lysed by four repeats of sonication at 80 kHz for 30 s. They were then filtered through 0.22- $\mu$ m PTFE  
199 syringe filters and aliquots of 450  $\mu$ l were diluted with 25  $\mu$ l of acetonitrile and 25  $\mu$ l of a  $^{13}$ C-caffeine  
200 (internal) standard solution (Sigma-Aldrich, Steinheim, Germany). These were injected in a liquid  
201 chromatography coupled with a quadrupole-time-of-flight mass analyser (LC-QTOF-MS) with an  
202 Agilent 1260 Infinity system (Agilent Technologies, Foster City, CA, USA) connected to a Triple TOF  
203 5600+ (Sciex Instruments, Foster City, CA, USA). The chromatographic separation was performed  
204 using a SB-C18 analytical column (3 mm x 250 mm, 5  $\mu$ m) [57]. TBZ transformation product analysis  
205 was carried out in the samples according to previous works [58, 59] and as described in the SI.

206

#### 207 **Modelling of enzyme-TBZ interactions.**

208 Selected ORFs which presented annotation relevant to aromatic compounds biodegradation (i.e. multi-  
209 component carbazole dioxygenase) and up-regulation in the presence of TBZ, shown in both meta-  
210 transcriptomic and meta-proteomic analysis, were computationally analyzed for possible ligand-protein  
211 interaction prognosis. Maximum common substructures between carbazole (the original substrate of  
212 the multi-component carbazole dioxygenase homologue identified as suspect catabolic enzyme in TBZ  
213 transformation) and TBZ (alternative substrate of carbazole dioxygenase, our study) were calculated



214 with the fmcSR v1.24.0 [60] as implemented by Rcp1 v1.18.1 [61]. The protein 3-dimensional structure  
215 models were calculated using SWISS-MODEL homology-based structure prediction approach [62].  
216 Docking of TBZ was performed using Autodock Vina v1.1.2 [63] and the Autodock Tools v4.2.6 [64],  
217 while Chimera v1.11.2 [65] was used for illustration of the results.

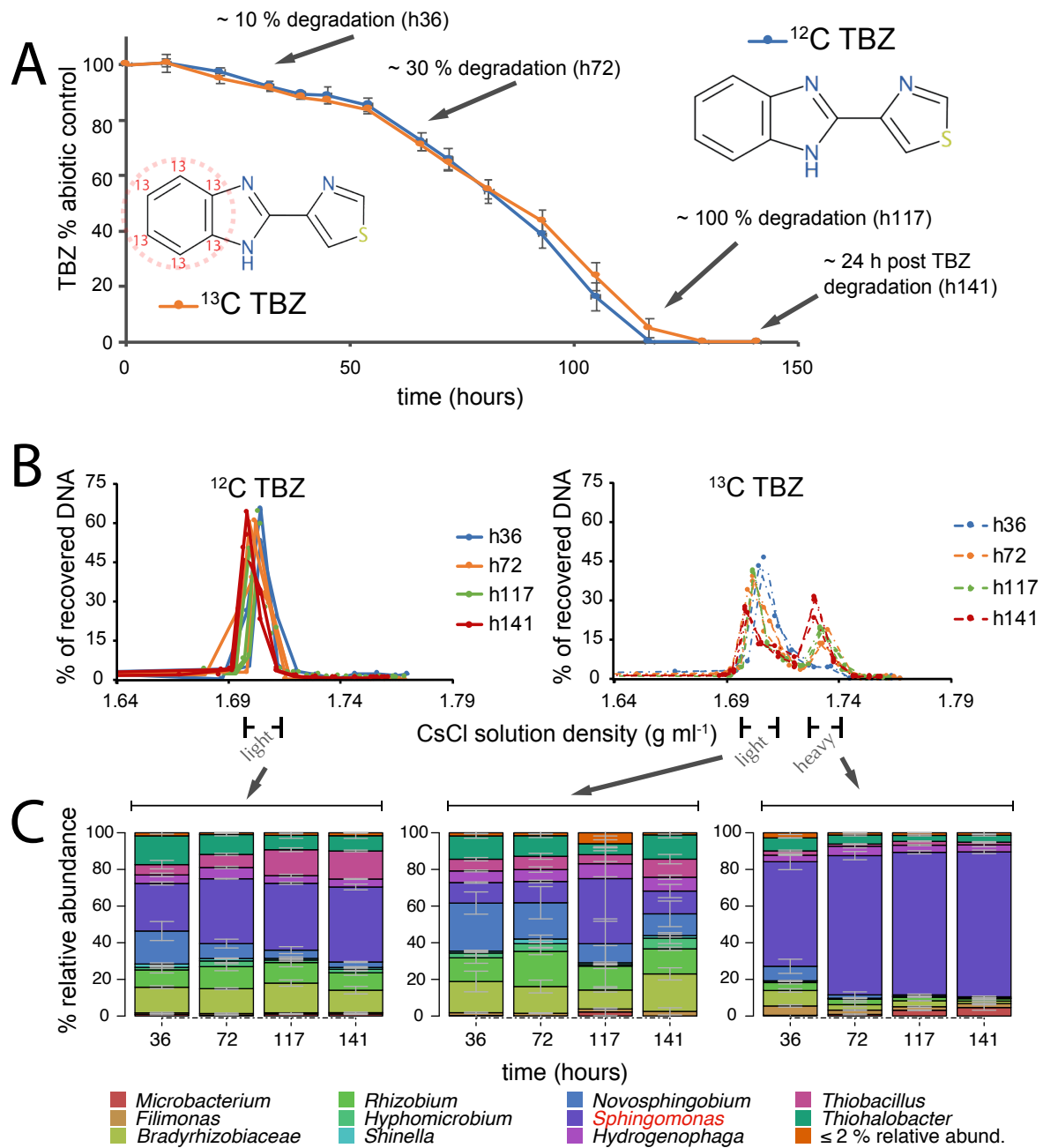
218

## 219 **Results**

### 220 **DNA-based SIP analysis of the bacterial consortium.**

221 The bacterial consortium was supplied with  $^{13}\text{C}$ -labelled and unlabelled TBZ as sole carbon source and  
222 the composition of the bacterial consortium was determined at four time-points along the degradation  
223 of TBZ (Figure 1A). DNA from the heavy ( $1.72 - 1.75 \text{ g ml}^{-1}$ ) and the light fractions ( $1.69-1.72 \text{ g ml}^{-1}$ )  
224 of the cultures supplemented with  $^{13}\text{C}$ -labelled TBZ (Figure 1B), and total DNA from the cultures  
225 supplemented with unlabelled TBZ was subjected to amplicon sequencing. In all treatments the  
226 bacterial consortium was dominated by the same nine main OTUs belonging to  $\alpha$ - (*Sphingomonas*,  
227 *Bradyrhizobiaceae*, *Rhizobium*, *Novosphingobium*, *Hyphomicrobium* and *Shinella*),  $\beta$ -  
228 (*Hydrogenophaga*, *Thiobacillus*) and  $\gamma$ -*Proteobacteria* (*Thiohalobacter*) (Figure 1C). However, their  
229 relative abundance varied in the heavy DNA fraction obtained from the  $^{13}\text{C}$ -TBZ supplied consortium,  
230 compared with the patterns observed in the corresponding light DNA fraction, and the consortium  
231 supplied with unlabelled TBZ (Figure 1C). Although the *Sphingomonas* OTU was dominant in all  
232 fractions and growth conditions, it entirely dominated the heavy DNA fraction of the community grown  
233 on  $^{13}\text{C}$ -labelled TBZ (>80 % relative abundance).

234



235

236 **Figure 1.** (A) The degradation patterns of unlabelled ( $^{12}\text{C}$ , blue line) and  $^{13}\text{C}$ -labelled TBZ (red line)

237 in MSMN inoculated with the bacterial consortium. Data are presented as % degradation relatively to

238 the non-inoculated abiotic control. Each value is the mean of three replicates  $\pm$  the standard deviation.

239 Arrows indicate the time points (and % degradation of TBZ) where amplicon sequencing analysis was

240 implemented; (B) Recovery of DNA after density gradient centrifugation of sample replicates

241 retrieved from the unlabelled TBZ supplemented culture (left) and the  $^{13}\text{C}$ -labelled-TBZ grown

242 cultures with the light (corresponding to the unlabelled TBZ sample peak CsCl solution densities of

243 1.69-1.72 g ml<sup>-1</sup>) and the heavy DNA fraction (corresponding to CsCl solution densities of 1.72-1.75  
244 g ml<sup>-1</sup>) separated along the CsCl density gradient (right panel); (C) The composition of the bacterial  
245 consortium (determined via 16S rRNA gene amplicon sequencing) in the different DNA fractions  
246 (unlabelled, light and heavy fraction of <sup>13</sup>C-labelled TBZ) described above, with stacked bars  
247 presenting the mean relative abundances of the OTUs among triplicates, and error bars showing the  
248 standard deviations (taxa with up to 2 % relative abundance in all samples were grouped together).

249

### 250 **Multi-omic and non-target MS analysis of TBZ transformation products**

251 We subsequently determined in a time-series experiment (i) the meta-genome/-transcriptome/-  
252 proteome of the bacterial consortium supplemented with TBZ or succinate (offered as a non-selective  
253 C source) and (ii) the transformation products produced during the degradation of TBZ by the  
254 consortium. These results allowed us to explore possible cross-feeding associations between members  
255 of the consortium, to identify their metabolic potential and genes/enzymes with possible role in the  
256 transformation of TBZ and eventually to propose a putative transformation pathway of TBZ.

257 **Metagenome analysis of the bacterial consortium:** The metagenome assembly resulted in 6,742  
258 contigs with an N50 of ~100 kb and an overall assembly length of ~98.5 Mbp (considering contigs >  
259 500 bp; Table S1), with the devoted sequencing effort sufficiently covering the existing diversity  
260 (Nonpareil based coverage of > 99% in all samples). Binning resulted in a total of 39 MAGs with 18 of  
261 them showing a minimum of 80 % genome completeness, and 7 of them having at least 90% quality  
262 according to MiGA and therein implemented indices [41], while contamination was 1.6 % on average  
263 ( $\pm 1.4$  % SD; Table S1). Amongst the assembled MAGs 11 showed mean relative abundance (in the  
264 three time points studied, 57, 96 and 120 h corresponding to 50%, 100% and 24h after complete  
265 degradation of TBZ) higher than 1% and all but one (MAG 8C, *Filimonas lacunae*, Bacteroidetes) were  
266 associated with  $\alpha$ -,  $\beta$ - and  $\gamma$ -*Proteobacteria*, in line with the SIP-amplicon sequencing data. The six  
267 most abundant MAGs accounted for over 72% of the assembled metagenome hits and identified as  $\gamma$ -  
268 *Proteobacterium* MAG 34A (mean abundance  $\pm$  standard deviation,  $21.8 \pm 7.9\%$ ), *Sphingomonas* MAG  
269 3X21F ( $17.9 \pm 7.1\%$ ), *Bradyrhizobiaceae* MAG 9B ( $16.3 \pm 9.7\%$ ), *Hydrogenophaga* MAG 23F ( $8.9 \pm$

270 4.2%), *Hydrogenophaga* MAG 19A ( $4.5 \pm 6.3\%$ ) and *Hydrogenophaga* MAG 13A ( $3.2 \pm 1.8\%$ ) (Table  
271 S1).

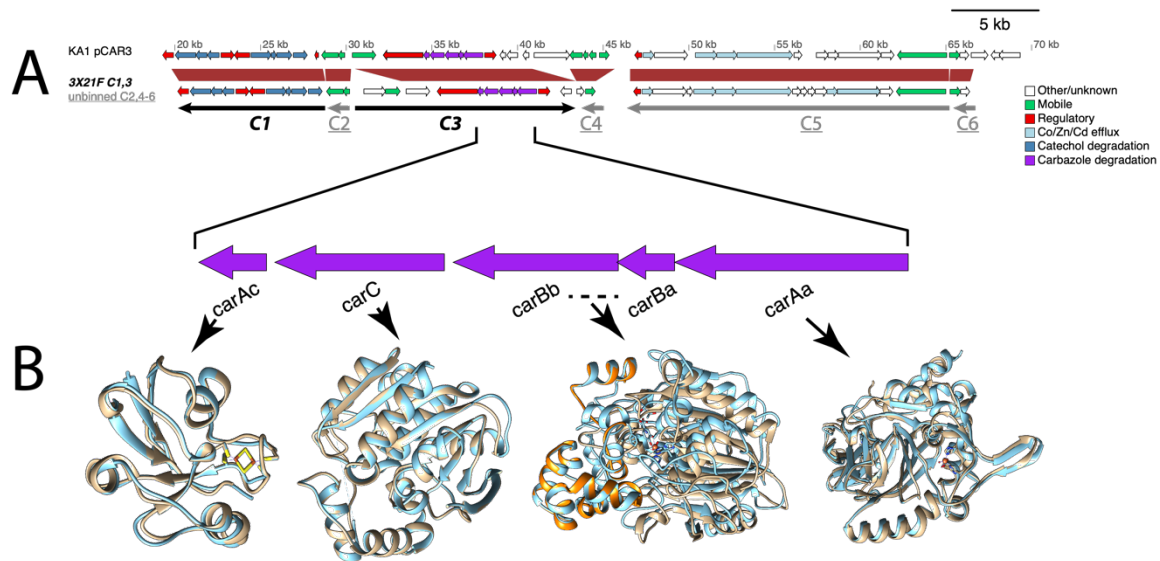
272

273 Translated ORF screening of the metagenome of the bacterial consortium against the AromaDeg  
274 database [43] indicated the presence of several genes scattered in the different MAGs and unbinned  
275 contigs with functional annotation associated with the aerobic degradation of monoaromatic (benzoate,  
276 genitsate, protocatechuate, salicylate, phthalate) and polyaromatic (biphenyl) hydrocarbons (Figure S1).

277 Of particular interest was the presence of a carbazole dioxygenase (*car*), with carbazole being a  
278 structural homologue of TBZ (Figure S2), and a catechol *ortho*-cleavage pathway (*cat*) operon on MAG  
279 3X21F contigs of *Sphingomonas*, which was identified as the main consumer of <sup>13</sup>C-TBZ (Table 1).

280 Comparative genomics between the *Sphingomonas* MAG 3X21F and other sphingomonad genomes  
281 revealed synteny between the genomic regions of *Sphingomonas* 3X21 MAG containing the *car/cat*  
282 operons and four unbinned contigs with a 50 kb region of the pCAR3 plasmid of the carbazole-  
283 degrading *Novosphingobium* sp. strain KA1 [66] (Figure 2A). Both *car* operons (in *Sphingomonas*  
284 3X21F MAG and in *Novosphingobium* sp. KA1) were missing *carAd* encoding the ferredoxin reductase  
285 component of carbazole dioxygenase. Instead we identified in another contig of the 3X21F MAG of  
286 *Sphingomonas* a ferredoxin reductase homolog gene *fdrI* (Table 1), known to be responsible for  
287 transferring electrons from NADH<sup>+</sup> to the reductase component of carbazole dioxygenase, CarAc,  
288 during carbazole transformation by *Novosphingobium* sp. KA1 [67].

289



Gene annotations per contig/contig-set of panel A in the same order and coloring as presented

**KA1 pCAR3:** *andR*, *catF*, *catJ*, *catI*, *catRll*, *catRl*, *catB*, *catC*, *catA*, *catD*, ORF31, *orfB*, *orfA*, ORF34, ORF35, *carAcI*, *carCI*, *carBbI*, *carBaI*, *carAaI*, *carRI*, ORF42, ORF43, ORF44, ORF45, *orfB*, *orfA*, ORF48, ORF49, ORF50, *czcD*, ORF52, *czcC*, *czcB*, *czcA*, ORF56, ORF57, ORF58, ORF59, ORF60, *tnpA*, *tnpR*, ORF63, ORF64, ORF65, ORF66

**3X21F C1,3 / unbinned C2,4-6:** *andR*, *pcaF\_2*, *pcaJ*, *pcaI*, *benR*, *benM*, *catB*, *catC*, *catA*, *catD*, *transposase*, *transposase*, hypothetical, IS5376 ATP-bind. prt., hypothetical, *TonB-dep rec*, *carAc*, *carC*, *carBb*, *carBa*, *carAa*, *carR*, hypothetical, hypothetical, *resolvase like*, *hmrR0*, *czcD*, *efeU*, hypothetical, *czcC*, *czcB*, *cnrA*, hypothetical, hypothetical, hypothetical, hypothetical, *czcD*, *cadA*, hypothetical, *hypothetical transposase*, *hypothetical transposase*, hypothetical

290

291 **Figure 2.** (A) Comparative analysis of a 50 kb stretch of the 255 kb long pCAR3 plasmid (upper arrow

292 panel) carried by *Novosphingobium* sp. KA1 (NCBI accession AB270530) [66] with the *car* and *cat*

293 operons found in the *Shingomonas* 3X21 MAG (lower arrow panel, contigs C1 and C3), and also the

294 unbinned contigs C2, C4, C5 and C6 of the assembled metagenome (NCBI accessions for C1-6:

295 QFCS01001188.1, QFCS01006733.1, QFCS01001185.1, QFCS01006070.1, QFCS01006598.1,

296 QFCS01006504.1). Red trapezoid shapes between upper and lower arrows panel denote homologous

297 regions between the bacterial consortium metagenome and pCAR3. Annotations of all the genes in the

298 two arrow panels are provided at the figure bottom, colored in consistency with the colors of the graphic

299 gene representations. (B) Structural alignments of the putative carbazole operon enzymes found in

300 *Shingomonas* 3X21 MAG with homologous characterized protein crystal structures deposited in the

301 protein databank (PDB; homologues are represented with the light blue crystal structures while our

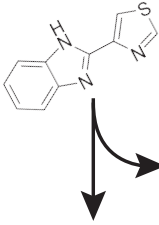
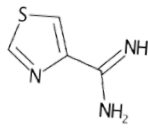
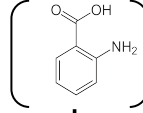
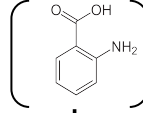
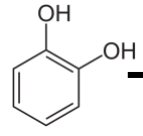
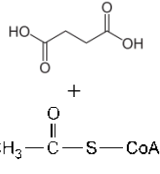
302 modeled protein structures have brown and orange colors – in the case of the CarBaBb dimer). Closest

303 PDB accession number per gene product: 1E9M for CarAc; 1B4U for CarBaBb; 3GKQ for CarAa; 1J1I

304 for CarC.

305

306 **Table 1.** Genes and enzymes with a putative role in the transformation of thiabendazole (TBZ) as  
 307 identified in the consortium metagenome. Their contig and operon residence, functional description,  
 308 the target compound transformed, and the relevant transformation products derived are presented. *Car*  
 309 operon encodes the enzymes responsible for the transformation of TBZ to thiazole-4-carboxamide  
 310 and catechol (directly or through the intermediate production of anthranilate) which is further  
 311 transformed, through the enzymes coded by the *cat* operon, to succinate and acetyl-CoA.  
 312

MAG	Contig accession	Operon	Protein	Functional description	Target compound	TP			
3X21F Sphingomonas	QFCS01001167.1	<i>car</i>	Fdrl	Ferredoxin--NAD(P)(+) reductase					
	QFCS01001185.1		TonB-dependent receptor	B12/siderophore receptor					
			CarAc	Ferredoxin					
			CarC	2-hydroxy-6-oxo-6-(2'-aminophenyl)hexa-2,4-dienoic acid hydrolase					
			CarBb	meta-cleavage subunit B					
			CarBa	meta-cleavage subunit A					
			CarAa	Carbazole 1,9a-dioxygenase, terminal oxygenase component					
			RspR	HTH-type transcriptional repressor					
unbinned	QFCS01005972.1	<i>and</i>	AndAd	Anthranilate 1,2-dioxygenase small subunit					
	QFCS01006510.1		AndAc	Anthranilate 1,2-dioxygenase large subunit					
	QFCS01006715.1		AndAa	Anthranilate 1,2-dioxygenase large subunit					
3X21F Sphingomonas	QFCS01001188.1	<i>and</i>	AndR	positive transcriptional regulator for anthranilate dioxygenase					
			<i>cat</i>	CatD			3-oxoadipate enol-lactonase 2		
				CatA			Catechol 1,2-dioxygenase		
				CatC			Muconolactone Delta-isomerase		
		CatB		Muconate cycloisomerase 1					
		BenM		HTH-type transcriptional regulator					
		PcaR		Pca regulon regulatory protein					
		PcaI	3-oxoadipate CoA-transferase subunit A						
		PcaJ	3-oxoadipate CoA-transferase subunit B						
		PcaF	Beta-ketoadipyl-CoA thiolase						

313

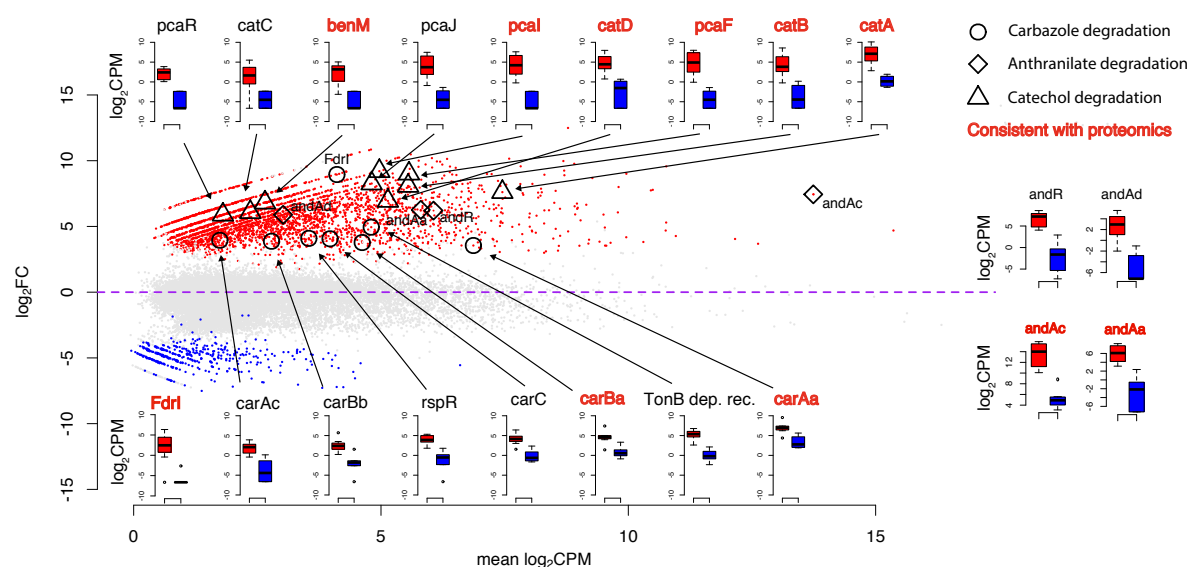
314

315 ***Meta-transcriptomic/-proteomic analysis of TBZ transformation genes:*** Metatranscriptomic analysis  
316 showed that 21,965 genes were differentially expressed with 2,986 being up-regulated and 408 being  
317 down-regulated in the presence of TBZ compared to succinate (Figure S3). Out of the several aromatic  
318 hydrocarbon transformation annotated genes present in the consortium metagenome, the *car* and *cat*  
319 operons present in the 3X21F MAG of *Sphingomonas* were significantly up-regulated in the presence  
320 of TBZ along with the putative ferredoxin reductase *fdrI*. (Figure 3). Furthermore, regulatory elements  
321 in the immediate vicinity of the *car* and *cat* operons (e.g. TonB dependent receptor and *rspR*  
322 transcriptional repressor at the *car* operon, and *benM/pcaR* at the *cat* operon) were also up-regulated in  
323 the presence of TBZ. We also observed a significant up-regulation of the different components of  
324 anthranilate dioxygenases (*andAcAdAa*) and their transcriptional regulator (*andR*) under TBZ  
325 supplementation (Figure 3). Apart from *andR* which was located upstream of the *cat* operon, all other  
326 anthranilate dioxygenase components were scattered in unbinned contigs (locus tags 04040, 06397,  
327 07193; Table 1).

328  
329 Corresponding meta-proteomic analysis of the bacterial consortium showed 2602 proteins to be  
330 differentially expressed in the two feeding conditions, 423 proteins being up-regulated and 652 down-  
331 regulated in the presence of TBZ (Figure S3). When focused on proteins with putative role in the  
332 transformation of TBZ, we noticed that the translated products of several of the genes of the *car* (*FdrI*,  
333 *CarAaBa*) and *cat* (*CatABD*, *PcaIF*) operons showed (consistent to the meta-transcriptomic data)  
334 significantly up-regulated profiles in the presence of TBZ (Figure 3). A consistent up-regulated profile  
335 in the presence of TBZ was also evident for anthranilate dioxygenase components *AndAaAc* (Figure  
336 3).

337





338

339 **Figure 3.** Differential expression profile of genes and enzymes of the bacterial consortium grown  
340 with thiabendazole (TBZ) or succinate. Data are presented as  $\log_2(\text{fold change})$  vs the means of the  
341  $\log_2(\text{copies per million reads} - \text{CPM})$  (MA) plot of the treatment-related gene differential expression  
342 according to RNA. The *car*, *cat* and *and* loci associated points are depicted with open circles,  
343 triangles and diamonds on the plots respectively. The expression boxplots in  $\log_2\text{CPM}$  values for  
344 genes with a putative role in the transformation of TBZ are also provided with arrows and/or symbols  
345 connecting them to the points of the MA plot. Genes/enzymes which showed consistent differentially  
346 expressed patterns at both metatranscriptomics and metaproteomics analysis are depicted with bold red  
347 letters according to the key.

348

349 Modeling and structural comparisons of the CarAaAcBaBbC components of the carbazole dioxygenase  
350 locus (Figure 2B) and of FdrI (Figure S4) found in the *Sphingomonas* 3X21F MAG with the  
351 corresponding components of the homologous characterized carbazole dioxygenase components of  
352 *Novosphingobium* sp KA1, showed nearly identical three-dimensional conformations. CarAa showed  
353 77% identities and 87% positives over the complete translated ORF length with the *Novosphingobium*  
354 sp. KA1 putative homologue and 30 identical out of the 32 amino acids around the active site pocket  
355 (Figure S5). The predicted CarAa active site pocket had similar affinity to carbazole ( $\Delta G = -7.5$  kcal  
356  $\text{mol}^{-1}$ ) compared to previously characterized CarAa enzymes (corresponding  $\Delta G$ s of  $-8.4$  and  $-7.4$  kcal



357 mol<sup>-1</sup> for *Janthinobacterium* and *Novosphingobium* sp. KA1 respectively), and a slightly lower affinity  
358 to TBZ (corresponding  $\Delta G$  values of -6.8 kcal mol<sup>-1</sup> compared to  $\Delta G$  values of -7 and -6.6 kcal mol<sup>-1</sup>  
359 for *Janthinobacterium* and *Novosphingobium* sp. KA1 respectively) (Figure S6).

360

361 **Transcriptional profile associations between consortium members.** We further investigated  
362 potential interdependencies and associations at functional level between the different members of the  
363 consortium. We performed a differentially-expressed-gene network analysis based on the  
364 metatranscriptomic data. We identified two dominant network substructures with connections between  
365 genes of *Sphingomonas* MAG 3X21F and the MAGs classified as *Hydrogenophaga* 23F,  
366 *Bradyrhizobiaceae* 9B, and unbinned contigs. Correlation analysis between the SEED functional gene  
367 categories of the genes comprising the network substructures, revealed a coincident expression of the  
368 genes contained in the putative *car* and *cat* operons of *Sphingomonas* MAG 3X21F and genes encoding  
369 cobalamin biosynthesis and its transmembrane transportation in the *Hydrogenophaga* MAG 23F  
370 (Figure 4A). TonB-dependent transporter genes which are responsive to siderophores, colisin and  
371 cobalamin [68], signaling genes with homology to the *fixLJ* two component systems (9 ORFs) and  
372 secondary messengers like cyclic AMP were all up-regulated in the presence of TBZ only in the  
373 *Sphingomonas* MAG 3X21F, although only cAMPs expression correlated with other MAGs (Figure  
374 4A).

375

376 We further investigated the completeness and the expression profile of the B12 biosynthesis and  
377 transportation systems encoded in the different MAGs (Figure 4B). Most major MAGs including  
378 *Sphingomonas* 3X21F contained several copies of the *btuB* and *btuF* genes encoding modules of the  
379 cobalamin transmembrane translocation system [73]. Regarding cobalamin biosynthesis  
380 *Hydrogenophaga* MAG23F carried copies of several of the genes necessary for the biosynthesis of the  
381 co-factor, while near complete B12 biosynthesis pathways were noted on other MAGs like  
382 *Hyphomicrobium* MAG 2A, *Shinella* MAG 7C and *Novosphingobium* MAG 5A (Figure 4B). On the  
383 other hand, *Sphingomonas* MAG 3X21F was amongst the poorest of the MAGs in genes associated  
384 with cobalamin biosynthesis. When the differential expression of the genes associated with the

385 biosynthesis and transportation of cobalamin in the different MAGs was recorded, we observed an up-  
386 regulation of the full array of the relevant genes in *Hydrogenophaga* MAG23F with concurrent up-  
387 regulation of genes *btuB* and *cobST* associated with transmembrane transportation and salvage of  
388 cobalamin respectively in *Sphingomonas* MAG 3X21F [69-71] (Figure 4B). In contrast we observed  
389 down-regulation of the corresponding *cob* genes in other MAGs (*Hyphomicrobium* 2A,  
390 *Novosphingobium*5A and *Shinella* 7C) with a populated biosynthetic pathway of cobalamin.

391

392 Assessment of keystone indices [54] based on the metatranscriptomic data network analysis further  
393 demonstrated the central role of the *Sphingomonas* MAG 3X21F among other MAGs (Figure S7). The  
394 genes of MAG 3X21F showed the highest degree, indirect degree (significance group a), and transitivity  
395 (highest significance groups; Figure S7), a relatively high closeness centrality (ranked 4<sup>th</sup> out of 9  
396 significance groups) and the lowest betweenness centrality values (8 out of 8 significance groups).

397

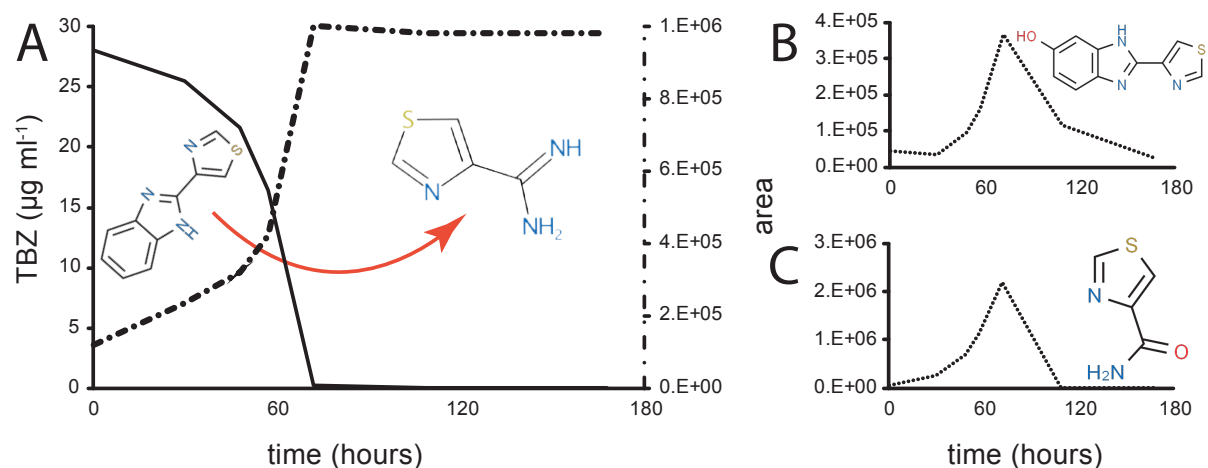


402 against the differentially expressed of other MAGs or genes on unbinned contigs of the same network  
403 groups. (B) Bubble plot showing the presence of cobalamin biosynthesis and transportation gene counts  
404 in the different MAGs of the bacterial consortium metagenome (left) and the expression profile (up- or  
405 down-regulated) of significantly differentially expressed genes when supplemented with TBZ or  
406 succinate (SCU) ( $\log_2(\text{TBZ}/\text{SUC})$ ; right). Per-panel provided keys explain significance of the plotted  
407 colors and bubble sizes.

408

409 **Non-target MS analysis of TBZ transformation products.** In the same time series experiment  
410 (experiment 2) we determined, via non-target MS analysis, the formation of potential transformation  
411 products of TBZ. The rapid degradation of TBZ was accompanied by the concurrent formation of a  
412 single major metabolic product with an MS spectrum of 127 m/z [14, 57-59] identified as 1,3-thiazole-  
413 4-carboxamide (Figure 5A). This product was not further transformed by the bacterial consortium.  
414 We also detected two other minor and transient transformation products in the bacterial culture  
415 identified as 5-OH-thiabendazole, with an MS spectrum of 218 (Figure 5B), and thiazole carboxamide,  
416 with an MS spectrum of 128 m/z (Figure 5C) (MS spectra given in our previous studies with TBZ [14,  
417 57-59]).

418



419

420 **Figure 5.** (A) The degradation of thiabendazole (TBZ) by the bacterial consortium (solid line,  $\mu\text{g ml}^{-1}$

421 <sup>1</sup>) and the formation (MS peak area) of the persistent transformation product 1,3-thiazole-4-

422 carboxamidine (dash-dotted line); (B) and (C) The formation and decay of the MS peak areas of the  
423 transient transformation products 5-OH-thiabendazole and thiazole-4-carboxamide respectively.

424

## 425 **Discussion**

426 Bacterial consortia often encompass complex metabolic and nutritional interactions which support  
427 effective pollutant degradation and their coherence. Working previously with a TBZ-degrading  
428 consortium we showed, via SIP-DGGE analysis at a single time point (taken upon completion of TBZ  
429 degradation) that a *Sphingomonas* sp. was the main TBZ degrader with the contribution of a  
430 *Hydrogenophaga* being suggested [14]. Here, by employing a time-series SIP-based amplicon  
431 sequencing approach we verified that *Sphingomonas* sp. is the sole member of the consortium involved  
432 in the transformation of TBZ, and no cross-feeding events of transformation products were observed.

433

434 We also assembled the metagenome of the bacterial consortium aiming to unravel the metabolic  
435 potential of its individual members. The consortium metagenome was composed of 18 major MAGs  
436 (with at least 80 % completeness); of those six were dominant, when grown on TBZ, with a rich arsenal  
437 of genes encoding the transformation of aromatic organic pollutants. Focusing on MAG 3X21F of  
438 *Sphingomonas* as the TBZ degrader of the consortium, we found genes with hits in the benzoate,  
439 biphenyl, extradiol, gentisate, LigB, protocatechuate and phthalate dioxygenase (super) families [43].  
440 Most interestingly, we noticed two DNA stretches approximating 20-kb, encompassing a *car* and a *cat*  
441 operon, both being significantly up-regulated during TBZ degradation according to meta-transcriptomic  
442 and meta-proteomic analysis, suggesting their involvement in the transformation of TBZ. Carbazole is  
443 an *N*-heterocyclic aromatic hydrocarbon, structurally similar to TBZ (Figure S2), found in fossil fuels  
444 and coal/wood combustion products, and it is used as a chemical feedstock for the production of dyes,  
445 reagents, explosives, insecticides, lubricants [72]. The carbazole skeleton is also present in natural  
446 alkaloids produced by the roots of several plants [73]. The high anthropogenic and biogenic exposure  
447 of several environments to carbazole skeleton explains the evolution of relevant catabolic degrading  
448 systems and their widespread occurrence amongst bacteria isolated from activated sludge and soil [74-  
449 76]. The *car* locus codes enzymes for the transformation of carbazole (and several other aromatic

450 pollutants) to catechol through the intermediate production of anthranilate [67]. The full transformation  
451 pathway includes the electron transfer from NAD(P)H through a ferredoxin reductase (FdrI/FdrII in  
452 *Novosphingobium* sp. KA1 [67] and CarAd in *Pseudomonas resinovorans* CA10 [77]) and a ferredoxin  
453 (CarAc) to the terminal oxygenase component (CarAa) which angularly dioxygenates carbazole.  
454 Following, a spontaneous cleavage takes place to form 2'-aminobiphenyl-2,3-diol, which is further  
455 cleaved by CarBaBb to a *meta*-cleavage product (2-hydroxy-6-oxo-6-(2'-aminophenyl)-hexa-2,4-  
456 dienoic acid), further hydrolyzed to anthranilate and 2-hydroxypenta-2,4-dienoic acid by CarC. The  
457 former is transformed to catechol by anthranilate dioxygenase AndAaAbAd and finally to succinate  
458 and acetyl Co-A via the catechol *ortho*-cleavage pathway. The *car* operon found in *Sphingomonas*  
459 MAG 3X21F comprised *carAaAcBaBbC*, lacking *carAd*. This is a common feature of other carbazole-  
460 degrading sphingomonads like *Sphingomonas* strain XLDN2-5 [78] and *Novosphingobium* sp.,  
461 GTIN11 [79] but not of *Pseudomonas* CA10 [80] and *Nocardioides aromaticivorans* IC177 [81] where  
462 *carAd* is part of the *car* operon. In the absence of *carAd* in its *car* operon, *Novosphingobium* sp. KA1  
463 plasmid pCAR3 contains genes coding for two ferredoxin reductases, FdrI/FdrII, located away from the  
464 two *car* operons of *Novosphingobium* sp. KA1 and acting as CarAd substitutes [67, 82]. Screening of  
465 *Sphingomonas* MAG 3X21F contigs lead to the identification of an FdrI homolog, which was highly  
466 up-regulated under TBZ at transcript and protein levels. The *fdrI* ORF found on the MAG of the main  
467 degrader, showed differential expression in the presence of TBZ, contradicting the previously reported  
468 constitutive expression in *Novosphingobium* sp. KA1 plasmid pCAR3 [82]; the difference in the  
469 expression pattern may be related to the range of the enzyme-dependent reactions in each tested case.  
470 Previous tests have also shown a broad range of activity compensation of FdrI/FdrII by spinach and  
471 *Escherichia coli* crude extract ferredoxin reductases by 96% and 4.5% respectively [77]. These results  
472 and the observed genetic organization of the relevant genes might suggest that *fdrI* is shared amongst  
473 several catabolic pathways, as previously proposed to be an evolutionary strategy of sphingomonads to  
474 maximize their catabolic potential and minimize their energetic burden [82, 83]. Alternatively, the  
475 pathway could be still under evolution [82]. The structural similarity of TBZ with carbazole, the  
476 remarkably relaxed specificity of carbazole dioxygenase which could transform a very wide range of  
477 polyaromatic pollutants (i.e., dibenzofuran, dibenzo-p-dioxin, biphenyl, naphthalene, dibenzothiophene,

478 diphenylamine) [67, 84] and its consistent up-regulation while growing with TBZ, suggest that  
479 carbazole dioxygenase is responsible for the initial step of the transformation of TBZ by the bacterial  
480 consortium. Further support of this is provided by the almost equivalent affinity of the CarAa found in  
481 3X21F MAG of *Sphingomonas* to carbazole and TBZ indicated by *in silico* docking tests.

482

483 Comparative analysis between the whole consortium metagenome and carbazole-degrading bacterial  
484 genomes showed high synteny of the *car/cat* operons with a 50 kb stretch of the pCAR3 plasmid  
485 encoding the full pathway for the transformation of carbazole in *Novosphingobium* sp. KA1 [66]. Both  
486 catabolic operons in MAG 3X21F and in *Novosphingobium* sp. KA1 were flanked by transposable  
487 elements suggesting that the *car/cat* genomic region of MAG 3X21F of *Sphingomonas* is a patchy  
488 construction acquired most probably by other sphingomonads through horizontal gene transfer.  
489 Sphingomonads are considered as "artists of biodegradation" due to their versatility in the degradation  
490 of organic pollutants [85-87] stemming from their remarkable capacity to exchange whole plasmids or  
491 mobile genetic elements to expand their catabolic repertoire [88, 89].

492

493 The *andAaAbAd* genes, although upregulated under the TBZ treatment, were not organized in the  
494 vicinity of the *car/cat* operons in MAG 3X21F, compared to the pCAR3 plasmid of *Novosphingobium*  
495 sp. strain KA1 where *and* genes were located closely upstream of the *cat* operon and in close proximity  
496 to the *car* operon [66]. Instead, in our case they were scattered in MAG-unassigned contigs implying  
497 that anthranilate is not produced during transformation of TBZ, in line with its lack of detection in the  
498 culture during TBZ degradation. However, it cannot be excluded that its presence in unbinned contigs  
499 might be associated with limitations of the metagenome assembly and binning methods with respect to  
500 the available sequencing technologies. For instance, the existence of several homologs of anthranilate  
501 dioxygenase throughout the consortium members (considering its role in the degradation of tryptophan  
502 and other aromatic compounds [84]) and its common localization in transposable elements [66, 78],  
503 may have resulted in population level repetitive regions which are usually recalcitrant to contiguousness  
504 in assembly, and also to coverage and sequence structure based binning [90]. In contrast, we found a  
505 complete putative *cat* operon composed of *catABCD* and *pcaIJF*, binned in MAG 3X21F of



506 *Sphingomonas* which was consistently upregulated, at both transcription and protein level, suggesting  
507 its operation in the transformation of catechol produced by the phenyl moiety of the benzimidazole ring  
508 of TBZ to tricarboxylic acid (TCA) cycle intermediates.

509

510 Considering all our meta-omic analysis, non-target MS analysis, current and previous isotopic ( $^{13}\text{C}$  and  
511  $^{14}\text{C}$ ) studies [14] we propose a transformation pathway of TBZ fully accomplished by *Sphingomonas*  
512 3X21F (Table 1): TBZ is initially cleaved at the imidazole moiety of the benzimidazole ring by  
513 carbazole dioxygenase CarAaAcFdr; this produces an unknown dioxygenated transient intermediate  
514 which is *meta*-cleaved by CarBaBb and hydrolyzed by CarC to 1,3-thiazole-4-carboxamide as a dead-  
515 end transformation product (in line with previous findings [14] and our non-target MS analysis), and  
516 catechol (directly or through the intermediate production of anthranilate). This is further transformed  
517 by *Sphingomonas* 3X21F (in line with the assimilation of the  $^{13}\text{C}$ -phenyl moiety of TBZ in the SIP  
518 analysis and previous radiorespirometric assays [15]) probably to the *ortho*-cleavage pathway terminal  
519 products acetyl-CoA and succinate, entering the TCA cycle.

520

521 We further looked for nutritional interdependencies between consortium members, beyond the  
522 transformation of TBZ, that might contribute to the consortium coherence. RNA-based network  
523 analysis revealed that certain functional features of *Sphingomonas* MAG 3X21F were highly correlated  
524 with *Hydrogenophaga* MAGs 23F, *Bradyrhizobiaceae* MAG 9B and unbinned contigs. Amongst them  
525 we observed a prominent positive correlative expression between cobalamin biosynthesis in  
526 *Hydrogenophaga* MAGs 23F and the catabolism of carbazole/catechol or the transportation system of  
527 cobalamin in *Sphingomonas* MAG 3X21F. Although several members of the consortium appear to  
528 possess a well populated cobalamin biosynthetic pathway, transcriptomic analysis revealed that only  
529 *Hydrogenophaga* MAG 23F mobilizes its cobalamin biosynthetic pathway (CobSTOQDP) and trans-  
530 membrane transportation, (BtuBF) in the presence to TBZ (Figure 6B). At the same time *Sphingomonas*  
531 MAG 3X21F, which is probably not capable of *de novo* biosynthesis of cobalamin, has activated its  
532 cobalamin transmembrane transportation system (BtuBF) and the *CobST* genes participating in the  
533 salvage pathway of cobamides [69, 70]. Since there are no known altruistic B12-producing bacteria



534 [22], our findings indicate a nutritional inter-dependency between *Sphingomonas* 3X21F and  
535 *Hydrogenophaga* 23F, complementing the probable B12 auxotrophy of the former with the B12  
536 prototrophy of the latter. Several studies have stressed the key role of cobalamin in shaping microbial  
537 communities [91], based on its key role as a co-factor in the reductive dehalogenation of organic  
538 pollutants [92] and other key metabolic reactions, and the evolutionary loss of the energetically costly  
539 B12 biosynthesis by most bacteria [23, 93, 94]. The missing cobalamin biosynthetic genes from the  
540 *Hydrogenophaga* MAG 23F could be the result of possible sequence divergence from characterized  
541 database genes or a low coverage of these regions by our sequencing effort.

542

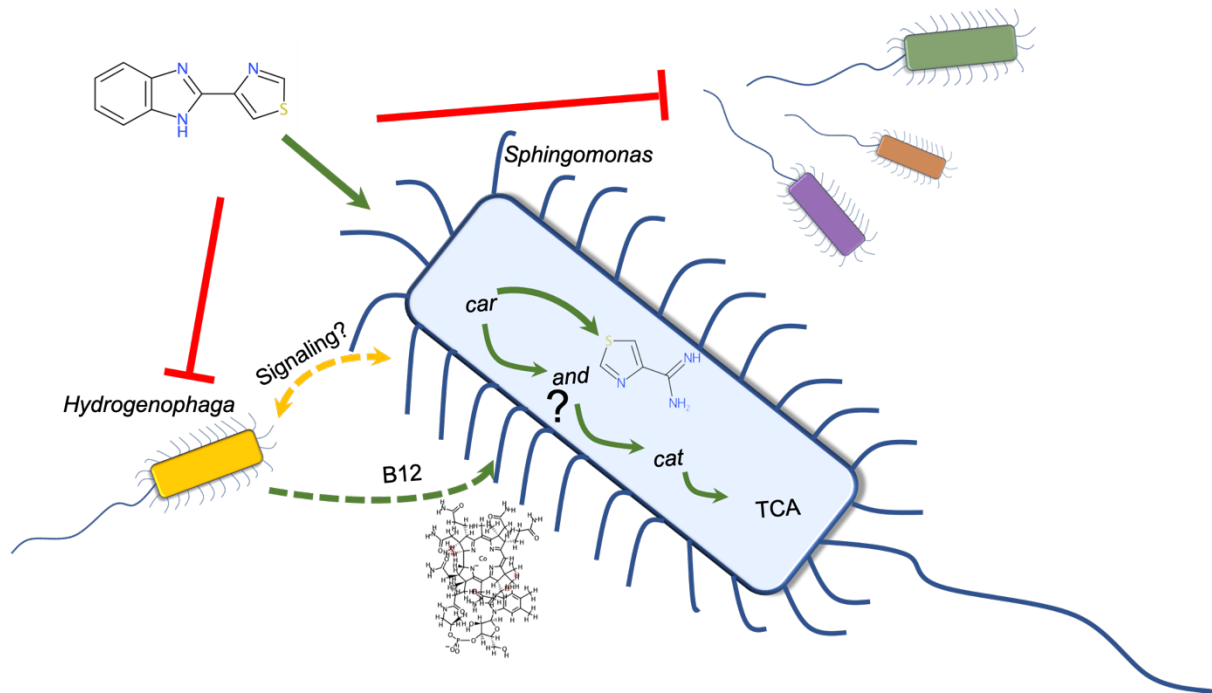
543 An interesting point is the specificity of the correlations between *Sphingomonas* MAG 3X21F and the  
544 *Hydrogenophaga* MAG 23F, given the presence of other *Hydrogenophaga* MAGs in the bacterial  
545 consortium metagenome which did possess cobalamin biosynthetic genes but showed no transcriptional  
546 correlation with the *Sphingomonas* MAG 3X21F. Hence, we looked for the activation of potential  
547 signaling mechanisms involving autoinducers or secondary messengers which might trigger this  
548 specific interaction. In the presence of TBZ we observed up-regulation of several *luxRI*-like two-  
549 component sensory-histidine-kinase/regulatory genes, annotated as *fixLJ* [95, 96] at the *Sphingomonas*  
550 MAG 3X21F, which did not appear to correlate with other members of the consortium. The *fixLJ* two  
551 component system is considered to sense oxygen in nitrogen fixing bacteria, yet, a broader sensory role  
552 of this two-component system was postulated in other bacteria (i.e. in the virulence of *Bulkhorderia*  
553 *dolosa*) [97, 98]. Cyclic AMPs, on the other hand, are involved mainly in intracellular signaling and  
554 were recently shown to participate in generic extracellular signaling, particularly during stress  
555 conditions [99, 100]. These two signaling modes were upregulated under the TBZ treatment and  
556 participated in the correlation network between the *Sphingomonas* MAG 3X21F and MAG 23F of  
557 *Hydrogenophaga*. These traits and our results render them suitable candidate systems mediating an  
558 interaction between the strains represented by the corresponding MAGs, which may have resulted in  
559 the MAG 23F derived cobalamin support of *Sphingomonas* (MAG 3X21F). A possible alternative mode  
560 for triggering cobalamin biosynthesis in *Hydrogenophaga* 23F could be associated with stress imposed  
561 by the presence of TBZ known to exert toxic effects on prokaryotes [101-103]. Besides *Sphingomonas*

562 MAG 3X21F, showing up-regulation of several stress-related genes when grown on TBZ (39 genes), a  
563 pattern often observed in pollutant-degrading bacteria during exposure to the target pollutant [104-106],  
564 *Hydrogenophaga* 23F was the only other MAG that mobilized a stress response, involving the up-  
565 regulation of a general stress response gene and a glutathione-S-transferase gene (locus tag:  
566 Bin\_23F\_Hydrogenophaga\_01167/03148). Oxidative stress elicitors have been shown to stimulate  
567 cobalamin production in bacteria [107]. Yet, this would also fail to explain on its own the specificity of  
568 the interaction, unless there are pronounced metabolic and functional differences among  
569 *Hydrogenophaga* consortium members, previously reported for *Hydrogenophaga* isolates [108], which  
570 enable this specialized interaction to occur.

571

## 572 **Conclusions**

573 We previously demonstrated the efficient degradation of the fungicide TBZ by a bacterial consortium  
574 and showed first evidence for the role of a *Sphingomonas* in TBZ degradation [14]. Here we provide  
575 unequivocal evidence that *Sphingomonas* is degrading TBZ without the involvement of any other  
576 member of the consortium. To achieve this, it employs a carbazole dioxygenase and a catechol *ortho*-  
577 cleavage operon, co-localized in a composite transposon most probably derived through horizontal gene  
578 transfer by other sphingomonads upon selection pressure imposed by TBZ contamination. In contrast  
579 to the lack of metabolic cross-feeding among consortium members in the transformation of TBZ, we  
580 observed a strong metabolic interdependency of the B12 auxotroph *Sphingomonas*, based on its  
581 assembled genome, with a *Hydrogenophaga* 23F which activates its cobalamin biosynthesis in response  
582 to TBZ degradation. Based on our results we propose a model, schematically presented in Figure 6, that  
583 describes the function of the TBZ-degrading consortium in line with the "black queen hypothesis"[109]:  
584 *Sphingomonas* 3X21F, is taking over the degradation of TBZ, relieving consortium members by a  
585 prokaryotic toxicant like TBZ [101-103]. In exchange for this, *Hydrogenophaga* 23F provides  
586 cobalamin to the auxotrophic *Sphingomonas* 3X21F ensuring the survival of the "black queen" of the  
587 consortium.



588

589 **Figure 6.** Proposed model describing the interactions between the members of the bacterial consortium  
590 driving the degradation of thiabendazole (TBZ). Green arrows indicate putative nutrient direction flows;  
591 yellow double arrows indicate signaling interactions; red blocked lines indicate possible inhibitory/toxic  
592 effects. *car*: carbazole-dioxygenase operon; *and*: anthranilate dioxygenase gene set; *cat*: catechol *ortho*-  
593 cleavage operon; TCA: tricarboxylic acid cycle.

594

#### 595 **Ethics approval and consent to participate**

596 Not applicable.

597

#### 598 **Consent for publication**

599 All the authors have seen and agree with the contents of this manuscript.

600

601 **Availability of data and material.** All sequence data are available at National Center for  
602 Biotechnology Information (NCBI) sequence read archive (SRA) under the bioproject accession  
603 number PRJNA466717 with: the metagenome assembly sequencing data accessible under the numbers  
604 SRR7135606-12; the RNA sequencing data and complete metadata are accessible through the NCBI

605 Gene Expression Omnibus (GEO) under the accession GSE134575 and SRA through accessions  
606 SRR9719617-34; the 16S rRNA gene amplicon sequencing data accessible under the numbers  
607 SRR9699065-175. The metagenome assembly contig set is publicly available at the NCBI Genbank  
608 database with the accession number GCA\_006513095.1.

609

### 610 **Competing interests**

611 The authors declare no competing interests.

612

### 613 **Funding**

614 Dr Vasileiadis is funded by the MSCA-IF-H2020 project EMIGRATE (Grant Agreement No.  
615 749463), Dr. C. Perruchon and Dr D.G. Karpouzas are supported by OMIC-ENGINE (MIS 5002636)  
616 funded by the Operational Program "Competitiveness, Entrepreneurship and Innovation" (NSRF  
617 2014-2020) and co-financed by Greece and the European Union (European Regional Development  
618 Fund). Protein mass spectrometry was done at the Centre for Chemical Microscopy (ProVIS) at the  
619 Helmholtz Centre for Environmental Research - UFZ, which is supported by European regional  
620 development funds (EFRE—Europe Funds Saxony) and the Helmholtz Association.

621

### 622 **Author's contributions**

623 KGD has conceived, designed and supervised all experiments along with the supervision of the  
624 drafting of the manuscript. PC participated in the experimental design, and the performance and  
625 supervision of the experiments. SB and AL designed the shotgun proteomics experiment and  
626 generated the data. SN and CA designed the SIP experiment and supervised its performance. PBP and  
627 AA designed the non-target MS analysis and generated the associated data. TM has participated in the  
628 experimental design and along with AL, CA and AA have provided feedback on the manuscript draft.  
629 VS has drafted the manuscript, performed all experiments except for the non-target MS analysis and  
630 the shotgun proteome analytical parts, performed the amplicon library prep for multiplex sequencing,  
631 the meta-genomics/transcriptomics/proteomics sample prep for sequencing or analysis, the TBZ

632 transformation products library preparation, the bioinformatics, the statistics and protein-ligand  
633 docking modeling, and participated in the experimental design.

634

### 635 **Acknowledgements**

636 The authors are thankful to Dr. Georgios E. Papadopoulos for his stewardship on the protein-ligand  
637 docking analysis.

638

### 639 **References**

- 640 1. D'Aquino S, Palma A, Angioni A, Schirra M. Residue Levels and Efficacy of Fludioxonil  
641 and Thiabendazole in Controlling Postharvest Green Mold Decay in Citrus Fruit When  
642 Applied in Combination with Sodium Bicarbonate. *J Agric Food Chem.* 2013; 61:296-306.
- 643 2. Panic G, Duthaler U, Speich B, Keiser J. Repurposing drugs for the treatment and control of  
644 helminth infections. *International Journal for Parasitology: Drugs and Drug Resistance.* 2014;  
645 4:185-200.
- 646 3. Özkay Y, Tunalı Y, Karaca H, Işıkdag İ. Antimicrobial activity of a new series of  
647 benzimidazole derivatives. *Archives of Pharmacal Research.* 2011; 34:1427.
- 648 4. Zhou Y, Xu J, Zhu Y, Duan Y, Zhou M. Mechanism of action of the benzimidazole fungicide  
649 on *Fusarium graminearum*: Interfering with polymerization of monomeric tubulin but not  
650 polymerized microtubule. *Phytopathology.* 2016; 106:807-13.
- 651 5. Abongwa M, Martin RJ, Robertson AP. A brief review on the mode of action of  
652 antinematodal drugs. *Acta Veterinaria.* 2017; 67:137-52.
- 653 6. Ccancapa A, Masiá A, Andreu V, Picó Y. Spatio-temporal patterns of pesticide residues in  
654 the Turia and Júcar Rivers (Spain). *Sci Total Environ.* 2016; 540:200-10.
- 655 7. Masiá A, Campo J, Vázquez-Roig P, Blasco C, Picó Y. Screening of currently used pesticides  
656 in water, sediments and biota of the Guadalquivir River Basin (Spain). *J Hazard Mater.* 2013;  
657 263:95-104.
- 658 8. European Food Safety Authority. Conclusion on the peer review of the pesticide risk  
659 assessment of the active substance thiabendazole. *EFSA J.* 2014; 12:3880.

- 660 9. Papadopoulou ES, Tsachidou B, Sułowicz S, Menkissoglu-Spiroudi U, Karpouzas DG. Land  
661 spreading of wastewaters from the fruit-packaging industry and potential effects on soil  
662 microbes: effects of the antioxidant ethoxyquin and its metabolites on ammonia oxidizers.  
663 *Appl Environ Microbiol.* 2016; 82:747-55.
- 664 10. US EPA. *Registration eligibility decision (RED): Thiabendazole.* 2002; EPA-738-F-02-002,  
665 US Environmental Protection Agency
- 666 11. European Commission. *Draft renewal assessment report prepared according to the*  
667 *Commission Regulation (EU) N.1141/2010, Second programme for the renewal of the*  
668 *inclusion of the following active substance under Regulation (EC) 1107/2009, Thiabendazole,*  
669 *Vol. I, Report and proposed decision.* 2013;
- 670 12. Campo J, Masiá A, Blasco C, Pico Y. Occurrence and removal efficiency of pesticides in  
671 sewage treatment plants of four Mediterranean river basins. *J Hazard Mater.* 2013; 263:146-  
672 57.
- 673 13. Walters E, McClellan K, Halden RU. Occurrence and loss over three years of 72  
674 pharmaceuticals and personal care products from biosolids–soil mixtures in outdoor  
675 mesocosms. *Water Res.* 2010; 44:6011-20.
- 676 14. Perruchon C, Chatzinotas A, Omirou M, Vasileiadis S, Menkissoglou-Spiroudi U, Karpouzas  
677 DG. Isolation of a bacterial consortium able to degrade the fungicide thiabendazole: the key  
678 role of a *Sphingomonas* phylotype. *Appl Microbiol Biotechnol.* 2017; 101:3881-93.
- 679 15. Perruchon C, Pantoleon A, Veroutis D, Gallego-Blanco S, Martin-Laurent F, Liadaki K, et al.  
680 Characterization of the biodegradation, bioremediation and detoxification capacity of a  
681 bacterial consortium able to degrade the fungicide thiabendazole. *Biodegradation.* 2017;  
682 28:383-94.
- 683 16. Breugelmans P, Barken KB, Tolker-Nielsen T, Hofkens J, Dejonghe W, Springael D.  
684 Architecture and spatial organization in a triple-species bacterial biofilm synergistically  
685 degrading the phenylurea herbicide linuron. *FEMS Microbiol Ecol.* 2008; 64:271-82.

- 686 17. Kim H, Kim D-U, Lee H, Yun J, Ka J-O. Syntrophic biodegradation of propoxur by  
687 Pseudaminobacter sp. SP1a and Nocardioides sp. SP1b isolated from agricultural soil. Int  
688 Biodeterior Biodegrad. 2017; 118:1-9.
- 689 18. Men Y, Feil H, VerBerkmoes NC, Shah MB, Johnson DR, Lee PKH, et al. Sustainable  
690 syntrophic growth of *Dehalococcoides ethenogenes* strain 195 with *Desulfovibrio vulgaris*  
691 Hildenborough and *Methanobacterium congolense*: global transcriptomic and proteomic  
692 analyses. ISME J. 2011; 6:410.
- 693 19. Hug LA, Beiko RG, Rowe AR, Richardson RE, Edwards EA. Comparative metagenomics of  
694 three Dehalococcoides-containing enrichment cultures: the role of the non-dechlorinating  
695 community. BMC Genomics. 2012; 13:327.
- 696 20. Xu X, Zarecki R, Medina S, Ofaim S, Liu X, Chen C, et al. Modeling microbial communities  
697 from atrazine contaminated soils promotes the development of biostimulation solutions.  
698 ISME J. 2019; 13:494-508.
- 699 21. Mee MT, Collins JJ, Church GM, Wang HH. Syntrophic exchange in synthetic microbial  
700 communities. Proc Natl Acad Sci. 2014; 111:E2149-E56.
- 701 22. Shelton AN, Seth EC, Mok KC, Han AW, Jackson SN, Haft DR, et al. Uneven distribution of  
702 cobamide biosynthesis and dependence in bacteria predicted by comparative genomics. ISME  
703 J. 2019; 13:789-804.
- 704 23. Zengler K, Zaramela LS. The social network of microorganisms — how auxotrophies shape  
705 complex communities. Nat Rev Microbiol. 2018; 16:383–90.
- 706 24. Mee MT, Wang HH. Engineering ecosystems and synthetic ecologies. Molecular  
707 BioSystems. 2012; 8:2470-83.
- 708 25. De Vrieze J, Boon N, Verstraete W. Taking the technical microbiome into the next decade.  
709 Environ Microbiol. 2018; 20:1991-2000.
- 710 26. Neufeld JD, Vohra J, Dumont MG, Lueders T, Manefield M, Friedrich MW, et al. DNA  
711 stable-isotope probing. Nat Protocols. 2007; 2:860-6.

- 712 27. Vasileiadis S, Puglisi E, Trevisan M, Scheckel KG, Langdon KA, McLaughlin MJ, et al.  
713 Changes in soil bacterial communities and diversity in response to long-term silver exposure.  
714 FEMS Microbiol Ecol. 2015; 91:fiv114.
- 715 28. Vasileiadis S, Puglisi E, Papadopoulou ES, Pertile G, Suciu N, Pappolla RA, et al. Blame it  
716 on the metabolite: 3,5-dichloraniline rather than the parent compound is responsible for  
717 decreasing diversity and function of soil microorganisms. Appl Environ Microbiol. 2018;  
718 84:e01536-18.
- 719 29. Parada AE, Needham DM, Fuhrman JA. Every base matters: assessing small subunit rRNA  
720 primers for marine microbiomes with mock communities, time series and global field  
721 samples. Environ Microbiol. 2016; 18:1403-14.
- 722 30. Apprill A, McNally S, Parsons R, Weber L. Minor revision to V4 region SSU rRNA 806R  
723 gene primer greatly increases detection of SAR11 bacterioplankton. Aquat Microb Ecol.  
724 2015; 75:129-37.
- 725 31. Hildebrand F, Tadeo R, Voigt A, Bork P, Raes J. LotuS: an efficient and user-friendly OTU  
726 processing pipeline. Microbiome. 2014; 2:30.
- 727 32. Author. entropart: An R package to measure and partition diversity. Journal. 2015; doi:  
728 10.18637/jss.v067.i08.
- 729 33. Oksanen J, Blanchet GF, Friendly M, Kindt R, Legendre P, McGilinn D, et al. Vegan:  
730 community ecology package. R package version 2.5-5. 2019. [https://CRAN.R-](https://CRAN.R-project.org/package=vegan)  
731 [project.org/package=vegan](https://CRAN.R-project.org/package=vegan)
- 732 34. R Core Team. R: A language and environment for statistical computing, reference index  
733 version 3.6.0. 2019. <http://www.R-project.org>
- 734 35. Albertsen M, Hugenholtz P, Skarshewski A, Nielsen KL, Tyson GW, Nielsen PH. Genome  
735 sequences of rare, uncultured bacteria obtained by differential coverage binning of multiple  
736 metagenomes. Nat Biotechnol. 2013; 31:533-8.
- 737 36. Rodriguez-R LM, Konstantinidis KT. Nonpareil: a redundancy-based approach to assess the  
738 level of coverage in metagenomic datasets. Bioinformatics. 2014; 30:629-35.



- 739 37. Rodriguez-R LM, Konstantinidis KT. Estimating coverage in metagenomic data sets and why  
740 it matters. *ISME J.* 2014; 8:2349-51.
- 741 38. Chevreux B, Pfisterer T, Drescher B, Driesel AJ, Müller WEG, Wetter T, et al. Using the  
742 miraEST Assembler for Reliable and Automated mRNA Transcript Assembly and SNP  
743 Detection in Sequenced ESTs. *Genome Res.* 2004; 14:1147-59.
- 744 39. Li D, Liu C-M, Luo R, Sadakane K, Lam T-W. MEGAHIT: an ultra-fast single-node solution  
745 for large and complex metagenomics assembly via succinct de Bruijn graph. *Bioinformatics.*  
746 2015; 31:1674-6.
- 747 40. Strous M, Kraft B, Bisdorf R, Tegetmeyer H. The binning of metagenomic contigs for  
748 microbial physiology of mixed cultures. *Front Microbiol.* 2012; 3:A410.
- 749 41. Rodriguez-R LM, Gunturu S, Harvey WT, Rosselló-Mora R, Tiedje JM, Cole JR, et al. The  
750 Microbial Genomes Atlas (MiGA) webserver: taxonomic and gene diversity analysis of  
751 Archaea and Bacteria at the whole genome level. *Nucleic Acids Res.* 2018; 46:W282-W8.
- 752 42. Seemann T. Prokka: rapid prokaryotic genome annotation. *Bioinformatics.* 2014; 30:2068-9.
- 753 43. Author. AromaDeg, a novel database for phylogenomics of aerobic bacterial degradation of  
754 aromatics. *Journal.* 2014; doi: 10.1093/database/bau118.
- 755 44. Leplae R, Lima-Mendez G, Toussaint A. ACLAME: A CLAssification of Mobile genetic  
756 Elements, update 2010. *Nucleic Acids Res.* 2010; 38:D57-D61.
- 757 45. Overbeek R, Olson R, Pusch GD, Olsen GJ, Davis JJ, Disz T, et al. The SEED and the Rapid  
758 Annotation of microbial genomes using Subsystems Technology (RAST). *Nucleic Acids Res.*  
759 2014; 42:D206-D14.
- 760 46. Zhao Y, Tang H, Ye Y. RAPSearch2: a fast and memory-efficient protein similarity search  
761 tool for next-generation sequencing data. *Bioinformatics.* 2012; 28:125-6.
- 762 47. Guy L, Roat Kultima J, Andersson SGE. genoPlotR: comparative gene and genome  
763 visualization in R. *Bioinformatics.* 2010; 26:2334-5.
- 764 48. Dobin A, Davis CA, Schlesinger F, Drenkow J, Zaleski C, Jha S. STAR: ultrafast universal  
765 RNA-seq aligner. *Bioinformatics.* 2013; 29:15-29.

- 766 49. Anders S, Pyl PT, Huber W. HTSeq - a Python framework to work with high-throughput  
767 sequencing data. *Bioinformatics*. 2015; 31:166–9.
- 768 50. Robinson MD, Smyth GK. Moderated statistical tests for assessing differences in tag  
769 abundance. *Bioinformatics*. 2010; 23:2881–7.
- 770 51. Robinson MD, McCarthy DJ, Smyth GK. edgeR: a Bioconductor package for differential  
771 expression analysis of digital gene expression data. *Bioinformatics*. 2010; 26:139-40.
- 772 52. Lund SP, Nettleton D, McCarthy Davis J, Smyth Gordon K. Detecting differential expression  
773 in RNA-sequence data using quasi-likelihood with shrunken dispersion estimates. *Statistical  
774 Applications in Genetics and Molecular Biology*. 2012; 11:A8.
- 775 53. Clauset A, Newman MEJ, Moore C. Finding community structure in very large networks.  
776 *Physical Review E*. 2004; 70:066111.
- 777 54. Berry D, Widder S. Deciphering microbial interactions and detecting keystone species with  
778 co-occurrence networks. *Front Microbiol*. 2014; 5:219.
- 779 55. Csardi G, Nepusz T. The igraph software package for complex network research.  
780 *InterJournal, Complex Systems*. 2006; 1695:1695.
- 781 56. Seidel K, Kühnert J, Adrian L. The complexome of *Dehalococcoides mccartyi* reveals Its  
782 organohalide respiration-complex Is modular. *Front Microbiol*. 2018; 9:A1130.
- 783 57. Sirtori C, Agüera A, Carra I, Sánchez Pérez JA. Identification and monitoring of  
784 thiabendazole transformation products in water during Fenton degradation by LC-QTOF-MS.  
785 *Anal Bioanal Chem*. 2014; 406:5323-37.
- 786 58. Campos-Mañas MC, Plaza-Bolaños P, Martínez-Piernas AB, Sánchez-Pérez JA, Agüera A.  
787 Determination of pesticide levels in wastewater from an agro-food industry: Target, suspect  
788 and transformation product analysis. *Chemosphere*. 2019; 232:152-63.
- 789 59. Martínez-Piernas AB, Plaza-Bolaños P, García-Gómez E, Fernández-Ibáñez P, Agüera A.  
790 Determination of organic microcontaminants in agricultural soils irrigated with reclaimed  
791 wastewater: Target and suspect approaches. *Anal Chim Acta*. 2018; 1030:115-24.
- 792 60. Horan K, Girke T, Backman TWH, Wang Y. fmcSR: mismatch tolerant maximum common  
793 substructure searching in R. *Bioinformatics*. 2013; 29:2792-4.

- 794 61. Chen AF, Cao D-S, Xiao N, Xu Q-S. Rcp1: R/Bioconductor package to generate various  
795 descriptors of proteins, compounds and their interactions. *Bioinformatics*. 2014; 31:279-81.
- 796 62. Waterhouse A, Bertoni M, Bienert S, Studer G, Tauriello G, Gumienny R, et al. SWISS-  
797 MODEL: homology modelling of protein structures and complexes. *Nucleic Acids Res*. 2018;  
798 46:W296-W303.
- 799 63. Trott O, Olson AJ. AutoDock Vina: improving the speed and accuracy of docking with a new  
800 scoring function, efficient optimization, and multithreading. *Journal of Computational*  
801 *Chemistry*. 2010; 31:455-61.
- 802 64. Morris GM, Huey R, Lindstrom W, Sanner MF, Belew RK, Goodsell DS, et al. AutoDock4  
803 and AutoDockTools4: Automated docking with selective receptor flexibility. *Journal of*  
804 *Computational Chemistry*. 2009; 30:2785-91.
- 805 65. Pettersen EF, Goddard TD, Huang CC, Couch GS, Greenblatt DM, Meng EC, et al. UCSF  
806 Chimera—A visualization system for exploratory research and analysis. *Journal of*  
807 *Computational Chemistry*. 2004; 25:1605-12.
- 808 66. Shintani M, Urata M, Inoue K, Eto K, Habe H, Omori T, et al. The *Sphingomonas* plasmid  
809 pCAR3 is involved in complete mineralization of carbazole. *J Bacteriol*. 2007; 189:2007-20.
- 810 67. Nojiri H. Structural and molecular genetic analyses of the bacterial carbazole degradation  
811 system. *Biosci, Biotechnol, Biochem*. 2012; 76:1-18.
- 812 68. Noinaj N, Guillier M, Barnard TJ, Buchanan SK. TonB-dependent transporters: regulation,  
813 structure, and function. *Annu Rev Microbiol*. 2010; 64:43-60.
- 814 69. Fang H, Li D, Kang J, Jiang P, Sun J, Zhang D. Metabolic engineering of *Escherichia coli* for  
815 de novo biosynthesis of vitamin B12. *Nat Commun*. 2018; 9:4917.
- 816 70. Author. Biosynthesis and use of cobalamin (B12). *Journal*. 2008; doi:  
817 doi:10.1128/ecosalplus.3.6.3.8.
- 818 71. Chimento DP, Mohanty AK, Kadner RJ, Wiener MC. Substrate-induced transmembrane  
819 signaling in the cobalamin transporter BtuB. *Nat Struct Biol*. 2003; 10:394-401.
- 820 72. Salam LB, Ilori MO, Amund OO. Properties, environmental fate and biodegradation of  
821 carbazole. *3 Biotech*. 2017; 7:111.

- 822 73. Schmidt AW, Reddy KR, Knölker H-J. Occurrence, biogenesis, and synthesis of biologically  
823 active carbazole alkaloids. *Chemical Reviews*. 2012; 112:3193-328.
- 824 74. Gieg LM, Otter A, Fedorak PM. Carbazole degradation by *Pseudomonas* sp. LD2: metabolic  
825 characteristics and the identification of some metabolites. *Environ Sci Technol*. 1996; 30:575-  
826 85.
- 827 75. Schneider J, Grosser RJ, Jayasimhulu K, Xue W, Kinkle B, Warshawsky D. Biodegradation  
828 of carbazole by *Ralstonia* sp. RJGII.123 isolated from a hydrocarbon contaminated soil. *Can J*  
829 *Microbiol*. 2000; 46:269-77.
- 830 76. Habe H, Ashikawa Y, Saiki Y, Yoshida T, Nojiri H, Omori T. *Sphingomonas* sp. strain KA1,  
831 carrying a carbazole dioxygenase gene homologue, degrades chlorinated dibenzo-p-dioxins in  
832 soil. *FEMS Microbiol Lett*. 2002; 211:43-9.
- 833 77. Nam J-W, Nojiri H, Noguchi H, Uchimura H, Yoshida T, Habe H, et al. Purification and  
834 characterization of carbazole 1,9a-dioxygenase, a three-component dioxygenase system of  
835 *Pseudomonas resinovorans* strain CA10. *Appl Environ Microbiol*. 2002; 68:5882-90.
- 836 78. Gai Z, Wang X, Liu X, Tai C, Tang H, He X, et al. The genes coding for the conversion of  
837 carbazole to catechol are flanked by IS6100 elements in *Sphingomonas* sp. strain XLDN2-5.  
838 *PLOS ONE*. 2010; 5:e10018.
- 839 79. Kilbane Ii JJ, Daram A, Abbasian J, Kayser KJ. Isolation and characterization of  
840 *Sphingomonas* sp. GTIN11 capable of carbazole metabolism in petroleum. *Biochem Biophys*  
841 *Res Commun*. 2002; 297:242-8.
- 842 80. Sato SI, Nam JW, Kasuga K, Nojiri H, Yamane H, Omori T. Identification and  
843 characterization of genes encoding carbazole 1,9a-dioxygenase in *Pseudomonas* sp. strain  
844 CA10. *J Bacteriol*. 1997; 179:4850-8.
- 845 81. Inoue K, Habe H, Yamane H, Nojiri H. Characterization of novel carbazole catabolism genes  
846 from Gram-positive carbazole degrader *Nocardioides aromaticivorans* IC177. *Appl Environ*  
847 *Microbiol*. 2006; 72:3321-9.

- 848 82. Urata M, Uchimura H, Noguchi H, Sakaguchi T, Takemura T, Eto K, et al. Plasmid pCAR3  
849 contains multiple gene sets involved in the conversion of carbazole to anthranilate. Appl  
850 Environ Microbiol. 2006; 72:3198-205.
- 851 83. Pinyakong O, Habe H, Yoshida T, Nojiri H, Omori T. Identification of three novel salicylate  
852 1-hydroxylases involved in the phenanthrene degradation of *Sphingobium* sp. strain P2.  
853 Biochem Biophys Res Commun. 2003; 301:350-7.
- 854 84. Nojiri H, Nam J-W, Kosaka M, Morii K-I, Takemura T, Furihata K, et al. Diverse  
855 oxygenations catalyzed by carbazole 1,9a-dioxygenase from *Pseudomonas* sp. Strain CA10. J  
856 Bacteriol. 1999; 181:3105-13.
- 857 85. Aylward FO, McDonald BR, Adams SM, Valenzuela A, Schmidt RA, Goodwin LA, et al.  
858 Comparison of 26 Sphingomonad Genomes Reveals Diverse Environmental Adaptations and  
859 Biodegradative Capabilities. Appl Environ Microbiol. 2013; 79:3724-33.
- 860 86. Verma H, Kumar R, Oldach P, Sangwan N, Khurana JP, Gilbert JA, et al. Comparative  
861 genomic analysis of nine *Sphingobium* strains: insights into their evolution and  
862 hexachlorocyclohexane (HCH) degradation pathways. BMC Genomics. 2014; 15:1014.
- 863 87. Zhao Q, Yue S, Bilal M, Hu H, Wang W, Zhang X. Comparative genomic analysis of 26  
864 *Sphingomonas* and *Sphingobium* strains: Dissemination of bioremediation capabilities,  
865 biodegradation potential and horizontal gene transfer. Sci Total Environ. 2017; 609:1238-47.
- 866 88. Stolz A. Degradative plasmids from sphingomonads. FEMS Microbiol Lett. 2014; 350:9-19.
- 867 89. Basta T, Keck A, Klein J, Stolz A. Detection and characterization of conjugative degradative  
868 plasmids in xenobiotic-degrading *Sphingomonas* strains. J Bacteriol. 2004; 186:3862-72.
- 869 90. Sangwan N, Xia FF, Gilbert JA. Recovering complete and draft population genomes from  
870 metagenome datasets. Microbiome. 2016; 4:A8.
- 871 91. Romine MF, Rodionov DA, Maezato Y, Osterman AL, Nelson WC. Underlying mechanisms  
872 for syntrophic metabolism of essential enzyme cofactors in microbial communities. ISME J.  
873 2017; 11:1434.

- 874 92. Yan J, Im J, Yang Y, Löffler FE. Guided cobalamin biosynthesis supports *Dehalococcoides*  
875 *mccartyi* reductive dechlorination activity. Philosophical Transactions of the Royal Society B:  
876 Biological Sciences. 2013; 368:20120320.
- 877 93. Garcia SL, Buck M, McMahon KD, Grossart H-P, Eiler A, Warnecke F. Auxotrophy and  
878 intrapopulation complementary in the ‘interactome’ of a cultivated freshwater model  
879 community. Mol Ecol. 2015; 24:4449-59.
- 880 94. Payne KAP, Quezada CP, Fisher K, Dunstan MS, Collins FA, Sjuts H, et al. Reductive  
881 dehalogenase structure suggests a mechanism for B12-dependent dehalogenation. Nature.  
882 2015; 517:513-6.
- 883 95. Wang S. Bacterial Two-Component Systems: Structures and Signaling Mechanisms. In:  
884 Huang C, editor. Protein Phosphorylation in Human Health: InTech; 2012.
- 885 96. Zschiedrich CP, Keidel V, Szurmant H. Molecular mechanisms of two-component signal  
886 transduction. J Mol Biol. 2016; 428:3752-75.
- 887 97. Schaefers MM, Liao TL, Boisvert NM, Roux D, Yoder-Himes D, Priebe GP. An oxygen-  
888 sensing two-component system in the *Burkholderia cepacia* complex regulates biofilm,  
889 intracellular invasion, and pathogenicity. PLoS Path. 2017; 13:e1006116.
- 890 98. Trastoy R, Manso T, Fernández-García L, Blasco L, Ambroa A, Pérez del Molino ML, et al.  
891 Mechanisms of bacterial tolerance and persistence in the gastrointestinal and respiratory  
892 environments. Clin Microbiol Rev. 2018; 31:e00023-18.
- 893 99. Green J, Stapleton MR, Smith LJ, Artymiuk PJ, Kahramanoglou C, Hunt DM, et al. Cyclic-  
894 AMP and bacterial cyclic-AMP receptor proteins revisited: adaptation for different ecological  
895 niches. Curr Opin Microbiol. 2014; 18:1-7.
- 896 100. Lin H, Hoffmann F, Rozkov A, Enfors S-O, Rinas U, Neubauer P. Change of extracellular  
897 cAMP concentration is a sensitive reporter for bacterial fitness in high-cell-density cultures of  
898 *Escherichia coli*. Biotechnol Bioeng. 2004; 87:602-13.
- 899 101. Slayden RA, Knudson DL, Belisle JT. Identification of cell cycle regulators in  
900 *Mycobacterium tuberculosis* by inhibition of septum formation and global transcriptional  
901 analysis. Microbiology. 2006; 152:1789-97.

- 902 102. Sarcina M, Mullineaux CW. Effects of tubulin assembly inhibitors on cell division in  
903 prokaryotes in vivo. FEMS Microbiol Lett. 2000; 191:25-9.
- 904 103. Kumar K, Awasthi D, Berger WT, Tonge PJ, Slayden RA, Ojima I. Discovery of anti-TB  
905 agents that target the cell-division protein FtsZ. Future Medicinal Chemistry. 2010; 2:1305-  
906 23.
- 907 104. Bers K, Leroy B, Breugelmans P, Albers P, Lavigne R, Sørensen SR, et al. A novel hydrolase  
908 identified by genomic-proteomic analysis of phenylurea herbicide mineralization by  
909 *Variovorax* sp. strain SRS16. Appl Environ Microbiol. 2011; 77:8754-64.
- 910 105. Vandera E, Samiotaki M, Parapouli M, Panayotou G, Koukkou AI. Comparative proteomic  
911 analysis of *Arthrobacter phenanthrenivorans* Sphe3 on phenanthrene, phthalate and glucose.  
912 Journal of Proteomics. 2015; 113:73-89.
- 913 106. Perruchon C, Vasileiadis S, Rousidou K, Papadopoulou E, Tanou G, Samiotaki M, et al.  
914 Metabolic pathway and cell adaptation mechanisms revealed through genomic, proteomic and  
915 transcription analysis of a *Sphingomonas haloaromaticamans* strain degrading ortho-  
916 phenylphenol. Scientific Reports. 2017; 7:6449.
- 917 107. Ferrer A, Rivera J, Zapata C, Norambuena J, Sandoval Á, Chávez R, et al. Cobalamin  
918 protection against oxidative stress in the acidophilic iron-oxidizing bacterium *Leptospirillum*  
919 group II CF-1. Front Microbiol. 2016; 7.
- 920 108. Yoon K-S, Tsukada N, Sakai Y, Ishii M, Igarashi Y, Nishihara H. Isolation and  
921 characterization of a new facultatively autotrophic hydrogen-oxidizing Betaproteobacterium,  
922 *Hydrogenophaga* sp. AH-24. FEMS Microbiol Lett. 2008; 278:94-100.
- 923 109. Morris JJ, Lenski RE, Zinser ER. The Black Queen Hypothesis: Evolution of Dependencies  
924 through Adaptive Gene Loss. mBio. 2012; 3:e00036-12.
- 925
- 926